

Article

Use of X-ray Microscopy for Confirmation of Crystallinity Detection in Amorphous Formulations by Electrospray Laser Desorption Ionization Mass Spectrometry Imaging

Kelsey K. Ramp ¹, Noah R. Dierckman ¹, Margaret A. Sperry ¹, Matthew E. Reuter ¹, Yongan Tang ² , Gregory K. Webster ² and Patrick A. McVey ^{1,*}

¹ Department of Chemistry and Physical Sciences, Marian University, Indianapolis, IN 46222, USA

² AbbVie Inc., North Chicago, IL 60064, USA; yongan.tang@abbvie.com (Y.T.); gregory.webster@abbvie.com (G.K.W.)

* Correspondence: pmcvety@marijan.edu; Tel.: +1-317-955-6481

Abstract: The use of mass spectrometry imaging for crystallinity detection offers improved matrix selectivity and sensitivity over the techniques, such as X-ray microscopy and Raman spectrometry, that are traditionally used with this work. Crystallinity is observed in electrospray laser desorption ionization mass spectrometry imaging (ELDI-MSI) as a high-intensity agglomeration of the analyte in a spatially resolved image. As this is an indirect method of crystallinity detection, confirmation of this method's ability to detect crystallization in amorphous formulations is needed by directly correlating observations of tablet crystallinity by ELDI-MSI to those of an established detection technique. Micro-computed tomography (micro-CT) has the necessary sensitivity for this investigation and is ideal for use in evaluating the correlation with crystallinity detection by ELDI-MSI. In this work, micro-CT followed by ELDI-MSI, in the same location on tablets of amorphous formulations of miconazole spiked with trace levels of crystalline miconazole, were analyzed. Crystals detected by ELDI-MSI as an agglomeration spatially matched with the detected crystals but were chemically unidentified by micro-CT. The results of this correlation study and a conclusion about the effectiveness of ELDI-MSI as a complimentary technique to indirectly detect crystallinity in enabling formations of an amorphous API are presented.

Keywords: electrospray laser desorption ionization; ELDI; mass spectrometry imaging; MSI; X-ray microscopy; micro-CT; crystallinity; pharmaceuticals; agglomeration



Citation: Ramp, K.K.; Dierckman, N.R.; Sperry, M.A.; Reuter, M.E.; Tang, Y.; Webster, G.K.; McVey, P.A. Use of X-ray Microscopy for Confirmation of Crystallinity Detection in Amorphous Formulations by Electrospray Laser Desorption Ionization Mass Spectrometry Imaging. *Crystals* **2023**, *13*, 1418. <https://doi.org/10.3390/crust13101418>

Academic Editors: Matteo Mori and Fiorella Meneghetti

Received: 25 August 2023

Revised: 7 September 2023

Accepted: 21 September 2023

Published: 24 September 2023



Copyright: © 2023 by the authors. Licensee MDPI, Basel, Switzerland. This article is an open access article distributed under the terms and conditions of the Creative Commons Attribution (CC BY) license (<https://creativecommons.org/licenses/by/4.0/>).

1. Introduction

As the pharmaceutical industry expands its portfolio to address unmet pharmaceutical needs, molecules that were historically not investigated due to solubility concerns are increasingly studied [1]. One approach in use today to positively increase the solubility and, thus, bioavailability of these active pharmaceutical ingredients (APIs) is the use of Amorphous Solid Dispersions (ASDs) [2,3]. For example, the use of Hot-Melt Extrusion (HME) typically dissolves an API in a liquefied polymer, where this mixture is then extruded to the desired size and shape. The extrudate is then cooled to form a solid solution where the amorphous API and polymer are uniformly dispersed [4].

The physical state of the API needs to be confirmed, as the crystallization of the amorphous drug during manufacturing and shelf life can affect bioavailability; therefore, quality control of the API in tablets is of high importance [5–7]. Crystallinity can be an issue for biopharmaceutical classification system (BCS) class II/IV drugs. Some drugs have differences in kinetic solubility between their different physical states [8,9]. Many crystalline forms of poorly soluble drugs go into solution even slower than their respective amorphous forms. In this case, the drug's kinetic solubility makes the amorphous form

more bioavailable and, thus, a more desirable physical state. In these enabling formulations, crystalline API could, therefore, be less bioavailable, negatively affecting a tablet's potency.

In the original work using electrospray laser desorption ionization mass spectrometry imaging (ELDI-MSI) for use in the crystalline-form detection of APIs in the presence of an amorphous drug, the data demonstrated that this imaging technique could be of use in studying enabling tablet formulations [10,11]. ELDI as an ionization source offers a matrix-free atmospheric pressure analysis, while mass spectrometry imaging (MSI) in this application optimizes the advantages of mass spectrometry instrumentation to spatially resolve the analytes on sample surfaces. The traditional spectroscopic methods used for this, such as X-ray imaging, can identify crystals within a tablet but cannot effectively discriminate between analytes and the matrix in the formulation [12,13]. Another spectroscopic technique, Raman spectroscopy, does not have the sensitivity needed to detect trace crystallinity in tablet formulations that is offered by mass spectrometry [8]. The selectivity of ELDI-MSI can selectively and simultaneously profile multiple APIs and other ingredients. Due to this, the capabilities and applications of MSI in the pharmaceutical industry for quality assurance are growing [8].

A crystalline API locality is detected in ELDI-MSI as a highly localized spectral intensity, or an agglomeration, of an analyte in the spatially resolved image. As this is an indirect method of crystallinity detection, this method's ability to detect crystallization in amorphous formulations needs to be confirmed by directly correlating observations of tablet crystallinity by ELDI-MSI with those of an established crystallinity detection technique. This application is below the detection capabilities of Polarized Light Microscopy (PLM) and typical XRPD methods [14]. While transmission electron microscopy combined with electron diffraction has the needed sensitivity, the destructive nature of the analysis and the lack of spatially resolved information for the crystalline API within the tablet matrix would not provide the needed correlation to the ELDI-MSI data. The kinetic solubility method can quantify API crystals at trace levels in tablet formations but is solely for bulk tablet determination [8]. Micro-computed tomography (micro-CT), or higher-resolution X-ray microscopy (XRM), has the necessary sensitivity for this investigation and is ideal for use in evaluating the correlation with crystallinity detection by ELDI-MSI, since it is non-destructive [15].

In this correlation study, enabling formulations of miconazole were spiked with varying trace levels of crystalline API and tableted. Miconazole was the chosen API due to its chemical structure containing multiple chlorine atoms, which allow for an observable contrast with micro-CT. The tablets were first imaged using micro-CT for crystallinity screening and then directly imaged in the same location and orientation with ELDI-MSI. The results of this correlation investigation to confirm whether ELDI-MSI can indirectly detect crystallinity in enabling formations of an amorphous API is presented.

2. Materials and Methods

2.1. Tablet Formulation

The ASD formulation of miconazole consisted of 12% drug load of miconazole, 1% surfactant polysorbate 80, and 87% copovidone. The 100 mg API control was made without any spiked crystalline API by mixing 833.3 mg ASD with 10 mg colloidal silicon dioxide, 151.7 mg dicalcium phosphate, and 5 mg magnesium stearate. Different crystalline spikes were made at 0.5%, 1%, and 2% (total drug load) of crystalline API by adding crystalline miconazole to the above formulation and appropriately lowering the amount of added ASD. Multiple replicates were created and tested at each crystalline percentage.

2.2. X-ray Microscopy

Tablets were first characterized using X-ray microscopy (micro-CT, Rigaku Nano3DX, Rigaku Americas Corporation, The Woodlands, TX, USA). The representative tablet sample was mounted on top of a thin rod, with the tablet's original, long, oval axis in the vertical direction. Scanning of the sample volume was performed using an L1080 lens with a 3.626

\times 2.719 mm field of view and a 3.2 μm slice width, as observed in Figure 1. The scan protocol included 180° rotation angle with 1200 steps, 6 s exposure time at each image step, and X-ray settings of 40 kV and 30 mA for characteristic copper X-ray sources. The scanned data were then reconstructed by the instrument's software with 8-bit reconstruction. The 3D visualization and segmentation were performed by Dragonfly software (Object Research Systems, Montreal, QC, Canada).

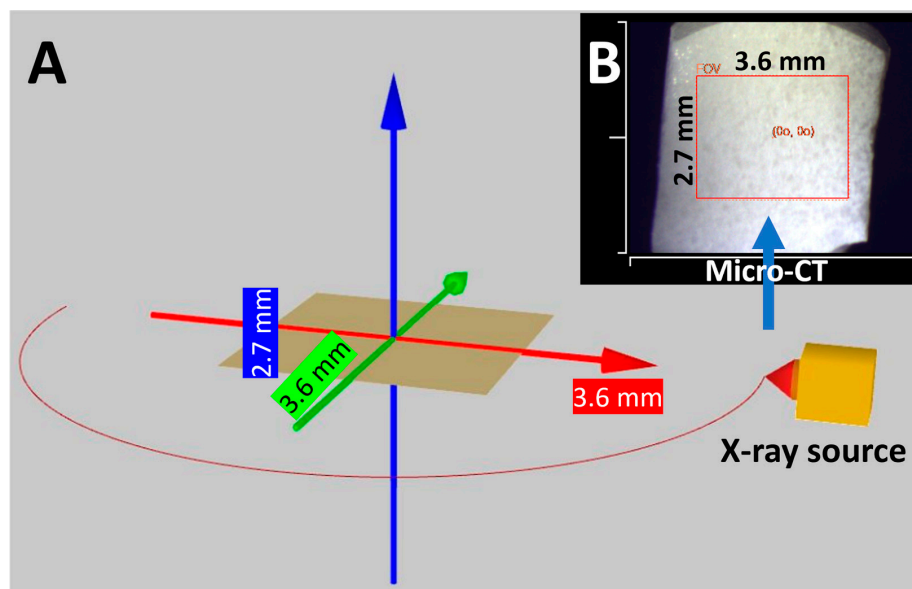


Figure 1. Image of sample during micro-CT scanning. (A) Schematic illustration of sample geometry during analysis. (B) Sample image at original position.

After analysis by micro-CT, tablets were mounted on glass slides with Loctite Fun-Tak Mounting Putty. They were then shipped to Marian University for ELDI-MSI analysis.

2.3. ELDI-MSI

A Thermo LTQ-XL linear ion trap mass spectrometer was operated in positive mode from 100 to 1000 m/z . The operating parameters were as follows: ESI voltage of +4.75 kV; ESI solution of 50:50 water:methanol with 0.1% formic acid (Fisher Chemical, 99.0%+ Optima grade); drying gas flow rate of 11 L/min; nebulizer gas pressure of 35 psi; inlet temperature of 100 °C; a nitrogen curtain gas flow rate of 6.0 L/h. An internally designed and modified electrospray ionization (ESI) source was combined with a Nd:YAG laser (Q-Spark-A50, Quantum Light Instruments, Ltd., Mokslininku str. 6A, Vilnius, Lithuania) to create the ELDI ion source. This source operated at atmospheric pressure. Spectra were summed for 0.25 s per image position. The LTQ XL was operated in Xcalibur and LTQ Tune Plus Version 2.7.0.1103 SP1.

The laser was operated on the fourth harmonic at 266 nm with a pulse repetition rate of 10 Hz and a <2 ns pulse width, with a nominal energy of 800 μJ /pulse (prior to focusing). A nominal spot size of ~25 μm was achieved as previously described [10,11]. Pill samples were carefully mounted on a 3D translation stage (Z825B, ThorLabs, Inc., Newton, NJ, USA) in the same orientation as used for analysis via micro-CT. No matrix was applied, and samples were analyzed at atmospheric pressure. Cross-sections of approximately 1.00 by 1.00 mm in the center of tablets were imaged to ensure that they were within the micro-CT dimensions. A lateral resolution of 25 μm was utilized, and, therefore, each MS-image pixel represents a total ablated volume of ~25 μm by 25 μm by 30 μm deep.

MS-images were generated as described in previous studies [10,11] using the same software packages [16,17]. MS-images were generated and then viewed using MSiReader V1.02 [18]. All generated MS-images used “linear squared” interpolation and the “Jet” color map for ease of interpretation. MS-images were then compared and overlayed with

micro-CT images of the same tablet in the same orientation with the exact dimensions. Slices from the micro-CT dataset were matched with depth-profiled MS-images.

3. Results

3.1. X-ray Imaging

The miconazole EDS results confirm that chlorine-rich API particles are generally elongated to correlate with micro-CT segmentation based on morphology and contrast, as observed in Figure 2. Miconazole displays a minor bright contrast in micro-CT images. The bright-white contrast observed in the micro-CT image is from dicalcium phosphate (DCP). While DCP is readily observable by micro-CT, it can be difficult to ascertain the location of the low-contrast signal from miconazole.

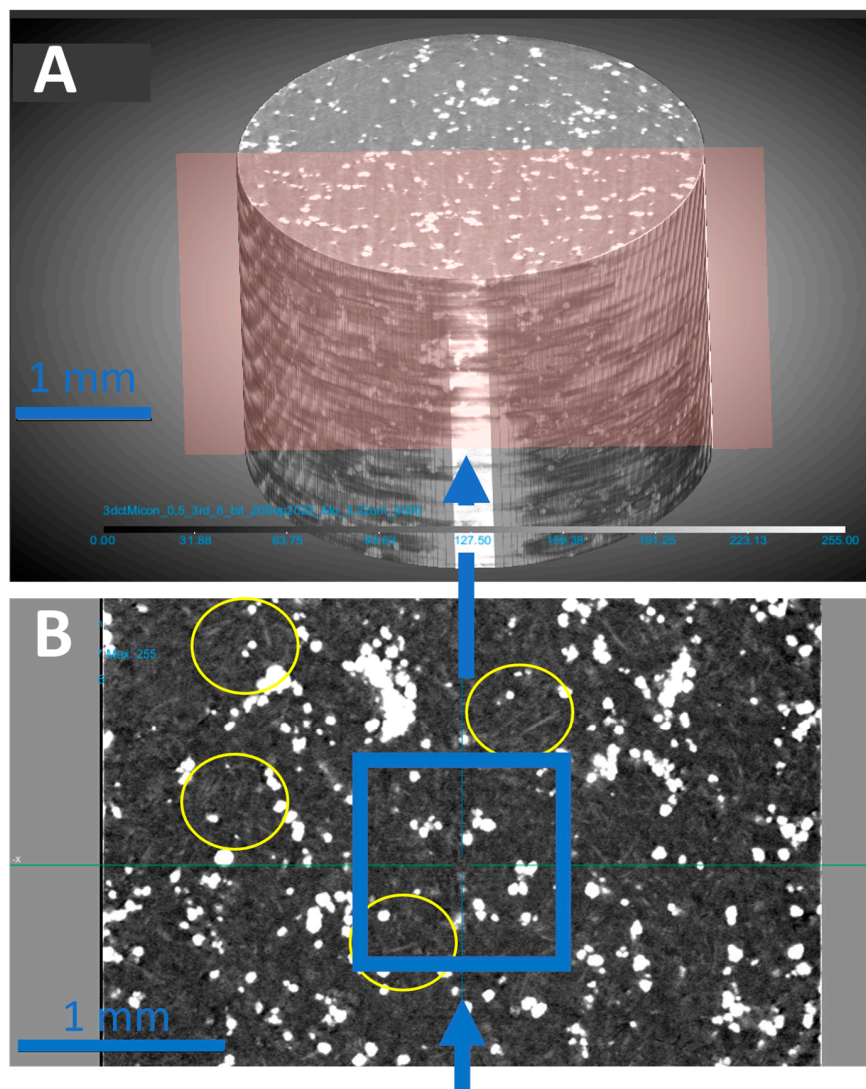


Figure 2. (A) The 3D micro-CT data for an imaged 0.5% crystalline miconazole API tablet. (B) A 2D slice image of micro-CT data highlighted in (A). Approximate MS-imaging dimensions given within blue square. Blue arrows show X-ray direction. Yellow circles show areas of crystalline API.

3.2. Mass Spectrometry Imaging Analysis

As observed in previous studies, the API was distributed throughout each analyzed surface layer of the tablet in the MS-images [10,11]. To confirm the identification of miconazole in the mass spectrum, the distribution of peaks between m/z 415 and m/z 423 were analyzed. Figure 3A shows the isotopic distribution, as observed in the mass spectra for miconazole, due to the presence of four chlorine atoms. A molecule with four chlorine

atoms should have an approximately 85:100:45:10% +2 isotope peak relative ion abundance, which is seen in Figure 3A [19]. Since ELDI is an inherently soft ionization technique, little fragmentation of miconazole was observed in the mass spectra. However, the observed peaks attributed to the fragmentation of miconazole include m/z 160.1 and 206.1 and their isotopes, which match with the literature [20]. The fragmentation ions from miconazole colocalized with intact miconazole ions and had similar intensity profiles. Figure 3B shows the typical observed distribution of miconazole in an MS-image. There was a low level of miconazole throughout every analyzed surface of the tablet. Figure 3C shows the process by which the low-level signal was filtered out. To do this, the threshold by which the miconazole signal is observed was raised in the MSiReader program. This filters out some of the low-level signal but maintains the high-intensity agglomeration. In Figure 3D, only the high-intensity signal is observed as the maximum threshold is raised once again, and the minimum threshold is also raised to remove the low-level signal from view. The minimum observable signal is labeled in each heatmap legend, with the legend of Figure 3D showing the increased threshold above zero. All MS-images shown are from miconazole at m/z 415.1. The MS-images at m/z 417.1, 419.1, and 421.1 are comparable to those in Figure 3.

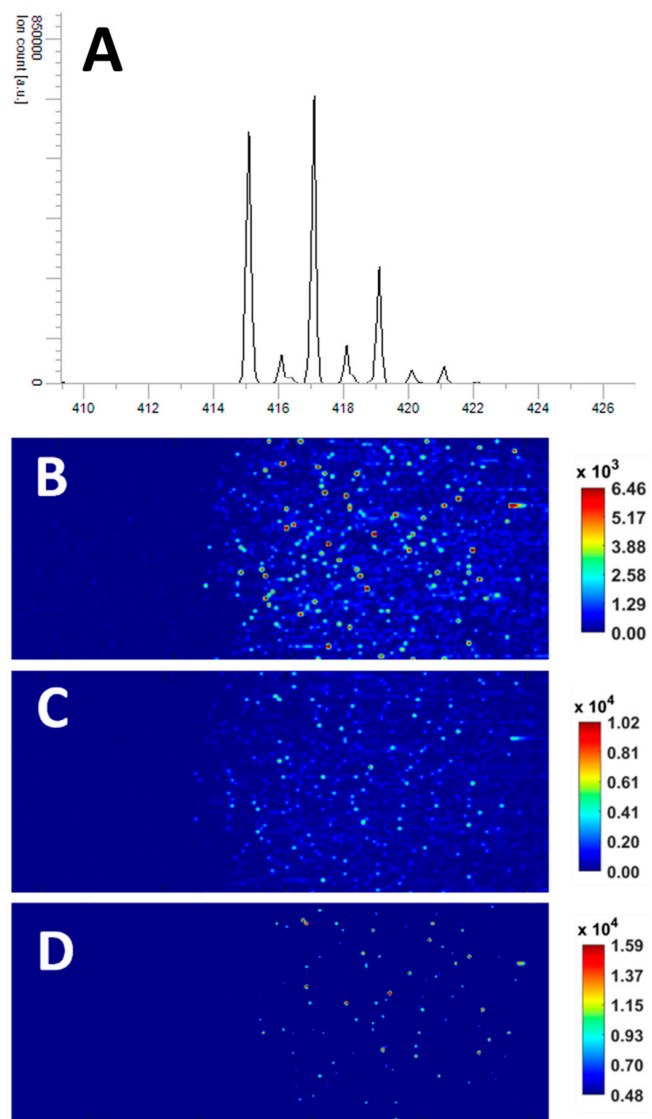


Figure 3. (A) Typical observed mass spectrum for miconazole $[M+H]^+$ and its isotopes. (B) MS-image of tablet with default min–max thresholds as determined by MSiReader. (C) MS-image of tablet with raised maximum threshold. (D) MS-image of tablet with raised minimum threshold and further raised maximum threshold.

3.3. MSI to X-ray Imaging Comparisons

To determine whether the miconazole signal observed by MSI matched with the minor bright contrast attributed to crystalline miconazole, only the high-intensity miconazole signal was overlaid with micro-CT, as seen in Figure 4. This was completed based on past observations, where the agglomerated API signal aligned with the areas of expected crystalline API. Figure 4 shows the typical MS high-intensity signal that is observed, which is colocalized with the low-contrast signal from micro-CT in a 1% crystalline miconazole tablet. The middle frame shows the MS-image at 50% transparency and overlaid on the micro-CT image for ease of visual analysis.

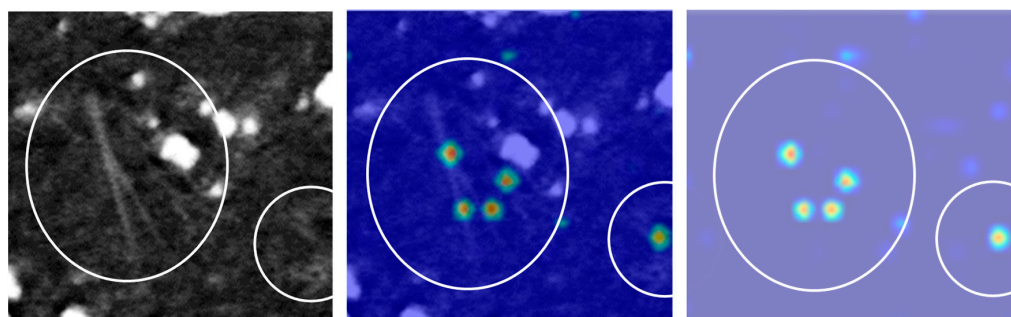


Figure 4. The left image shows micro-CT image of low-contrast elongated signal from crystalline miconazole. The right image shows the MS-image of the same area. Middle image is an overlay of the MS-image over the micro-CT image displaying colocalization of signal.

Similarly, in Figure 5, the MS-image of the high-intensity miconazole (2% crystalline miconazole) observed at m/z 415.1 is in the right frame. The left frame shows the micro-CT image of the same depth slice. The middle frame shows the MS-image at 50% transparency and overlaid on top of the micro-CT image. Figure 5 shows a larger area in which multiple different crystals are identified as miconazole. As seen in both Figures 4 and 5, the high-intensity signal is observed colocalizing with the low-contrast signal seen by micro-CT. Due to the process of removing the lower-intensity signal (as shown in Figure 3), the MS-images only colocalize with a part of the low-contrast signal, usually in highly localized spots. This matches with the results on previously studied APIs, where the crystalline API partially aligned with spots of API “agglomeration”.

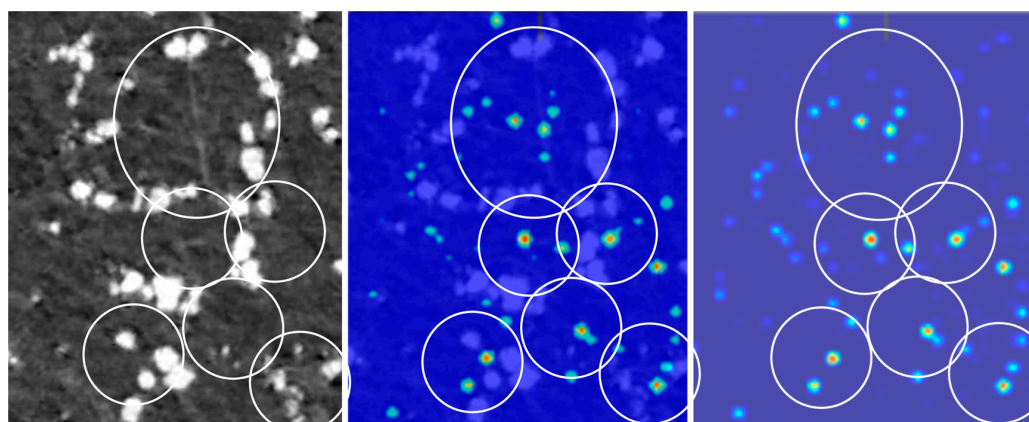


Figure 5. The left image shows micro-CT image of low-contrast signal from crystalline miconazole. The right image is the MS-image of the same area. Middle image is an overlay of the MS-image over the micro-CT image displaying colocalization of signal. Areas of high-intensity miconazole as detected by MS are circled.

Figure 6 shows a 0.5% crystalline miconazole tablet with a similar distribution of the high-intensity signal colocalizing with the low-contrast micro-CT signal. The overall micro-

CT image is shown with the MS-image overlaid, displaying the typical imaging dimensions. This image highlights the colocalization of high-intensity spots with the low-contrast signal, as observed in the circled areas on the overlay image. Other high-intensity spots observed in the MS-image could be observed in micro-CT slices immediately before or after the micro-CT slice that is shown. Figure 6 is a representation of the MSI results that were taken and analyzed relative to micro-CT.

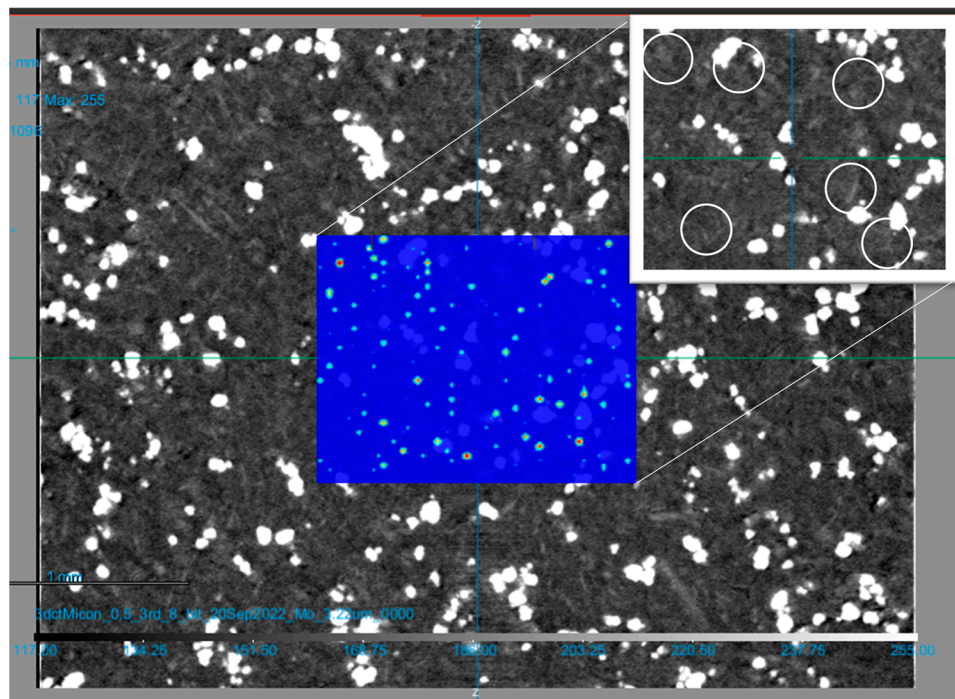


Figure 6. Micro-CT slice of a 0.5% crystalline miconazole tablet with the corresponding MS-image overlaid. The micro-CT insert in the top right of the figure shows the area under the MS-image with the white circles showing major areas of agglomeration.

4. Discussion

Considering the drug load of the tablet (10% of the overall weight), the low-intensity miconazole signal observed throughout the tablet by mass spectrometry should be expected. The high-intensity MS signal and areas of the low-contrast micro-CT signal consistently colocalized in all replicates. This shows that the MS-images are accurately predicting the locations of crystalline miconazole through highly localized spikes of miconazole signal intensity. The increase in MS intensity observed in the low-contrast areas gives insight into where crystalline miconazole is located, and the observed low-intensity MS signal colocalizes with entire crystalline structures. However, the amorphous miconazole observed throughout the tablet with a near-equal distribution overlaps with other areas of the expected crystalline miconazole signal. Therefore, eliminating the low-intensity signal, which filters out any signal from amorphous miconazole, allows crystalline API locations to be determined without interference.

A good representation of the typical observations of miconazole crystals, as observed both in the MS-images and by micro-CT, is shown in Figure 4. With the low-intensity MS signal filtered out, only partial colocalization is observed with the elongated miconazole crystals. However, the agglomeration of miconazole observed by MSI consistently matches with the low-contrast signal. In Figure 5, large miconazole crystals are observed corresponding to multiple agglomerated spots in the MS-image. Some areas identified as crystalline miconazole by MSI were not elongated structures but rather broad areas of the low-contrast signal in the micro-CT image. This agreed with the X-ray elemental analysis.

In some images, such as in Figure 5 in the leftmost circle, there is little-to-no observable contrast in the micro-CT image where the high-intensity MSI signal is observed. This is likely due to the sampling depth of MSI being greater than the representative micro-CT images. Micro-CT has a slice width of 3.2 μm , while MSI has a sampling depth of approximately 25–30 μm . Since miconazole crystals are much larger than 3.2 μm , they can show up in multiple micro-CT slices depending on their directionality in the tablet relative to sampling by X-ray. The low-contrast signal was observed in these high-intensity areas in subsequent micro-CT slices, and little-to-no high-contrast DCP signal was observed in these areas. Binning multiple micro-CT scans together to alleviate this issue resulted in blurry images that lost all contrast.

In general, some of the signal comes close to DCP crystals but is located around said crystals in a low-contrast signal area. Figure 6 shows an example of the partial colocalization with a DCP crystal in the bottom-left quadrant of the overlaid MS-image. This is another example of the low-contrast signal observed in this area in subsequent micro-CT slices. Figure 6 represents a typical MS-image-to-micro-CT overlay and comparison.

MSI could not give information about what the crystallinity percentage was inside the different tablet blends. Although there was a general difference across replicates between the 2% crystalline blend and the 0.5% crystalline blend, it was not consistent. This is likely due to the relatively small sampling area in this study, as shown in Figure 6. However, even when entire tablets were imaged to determine the efficacy of the technique for crystalline identification and quantification, we did not find correlations between the blended crystalline miconazole percentage and the total number of high-intensity spots observed. This same phenomenon, however, was observed by micro-CT as well for the observable low-contrast signal. Therefore, it is likely an issue with the tablet blend and not with either technique used for crystal detection.

The overall percentages of crystalline API in these tablet blends were very low, and MSI and micro-CT both successfully located crystalline miconazole. Virtually no high-intensity signal was observed in control tablets without blended crystalline miconazole, which agreed with the micro-CT results (see Supplemental Figure S1). Therefore, the technique is currently useful for localizing and detecting API crystals but not for quantifying crystalline API. However, this is an inherent issue with MSI in general, as quantification proved to be difficult due to several factors [21].

It could be expected to observe a high-intensity MS signal throughout the entirety of the crystals, as seen by micro-CT; however, this was not observed. This is partially due to the MS signal filtering process used to isolate only the high-intensity MS signal. However, a key aspect is the orientation of each individual miconazole crystal relative to the laser-ablation process. This would have a direct influence on the signal observed in each crystal. The orientation of the individual molecules within the crystalline packing structure relative to the laser is also a factor. Once a crystal is successfully ablated, the overall crystal structure is no longer intact, and, therefore, the factors that lead to the highly agglomerated signal are potentially no longer there.

In summary, the agglomerated spots of miconazole, as seen in the MS-images, gave consistent insight into the locations of miconazole crystals when compared to micro-CT. When the laser-ablation process struck a crystal at the correct orientation, these agglomerated spots were observed. Virtually no agglomerated spots were observed in tablets without blended crystalline miconazole. Overlays of MS-images on top of the micro-CT results for the same slice allow for spatial assignments of crystals, as seen in Figures 4–6.

5. Conclusions

These results show that ELDI-MSI's identification of crystallinity correlates to that of micro-CT. Therefore, the technique can be especially useful as a tool for low-level crystallinity determination and can provide confirmation of molecular identifications for the micro-CT results. This also shows the applicability of MSI to study potential crystalline API in regions where micro-CT cannot be used. MSI can be a tool to identify areas of

crystalline API through the high-intensity signal, in conjunction with X-ray imaging or similar spectroscopic methods.

Further investigations into additional APIs are needed to determine the consistency of the results when comparing MSI to micro-CT. While certain drugs may not appear as an observable contrast signal in micro-CT and, therefore, may not be directly comparable to a representative MS-image, MSI can still be utilized to determine the potential presence and localities of crystalline API. A careful data analysis technique is needed, as multiple micro-CT “slices” can correspond to just one MS-image. This could be mitigated by a smaller laser sampling depth or an improvement in the binning process of multiple micro-CT slices.

Future studies will test other APIs. Currently, tablets containing clotrimazole are undergoing analysis via both micro-CT and ELDI-MSI. Clotrimazole was chosen because it has one chlorine atom per molecule compared to four for miconazole and, therefore, has a less observable contrast by micro-CT. Quercetin tablets are also being analyzed to determine the efficacy of the technique for molecules that are non-observable via X-ray. These APIs were chosen to determine the robustness of the methodology.

Additional method improvements are also ongoing. Enhanced spatial resolution would potentially allow for a greater differentiation of the high-intensity MSI signal colocalizing with crystalline API. Increased sensitivity would also allow for a lower laser energy output and, therefore, a smaller sampling depth closer to the individual slice width of micro-CT. Current studies are working on a 100% increase in the spatial resolution down to 12 μm and an improved pneumatically assisted ESI design to increase sensitivity.

Supplementary Materials: The following supporting information can be downloaded at <https://www.mdpi.com/article/10.3390/crust13101418/s1>.

Author Contributions: Conceptualization, P.A.M. and G.K.W.; methodology P.A.M.; validation, K.K.R., N.R.D., M.A.S. and M.E.R.; formal analysis, K.K.R., N.R.D., M.A.S., M.E.R., Y.T. and P.A.M.; investigation, K.K.R., N.R.D., M.A.S. and Y.T.; writing—original draft preparation, G.K.W., Y.T. and P.A.M.; writing—review and editing, K.K.R., N.R.D., P.A.M., G.K.W. and Y.T.; visualization, K.K.R., P.A.M. and Y.T.; supervision, P.A.M.; project administration, G.K.W. and P.A.M.; funding acquisition, G.K.W. and P.A.M. All authors have read and agreed to the published version of the manuscript.

Funding: This research was funded by AbbVie Inc. under grant number 104796.

Data Availability Statement: Additional data of replicates performed on standard tablets are available upon written request to the corresponding author.

Acknowledgments: The authors would like to thank the Marian University Office of Sponsored Programs & Research for its support. The authors would also like to thank AbbVie Inc. for its support of undergraduate research.

Conflicts of Interest: The authors declare no conflict of interest. G.K.W. and Y.T. are employees of AbbVie and may own AbbVie stock. P.A.M. is an employee of Marian University. K.K.R., N.R.D., M.A.S., and M.E.R. were students at Marian University at the time of the study. AbbVie sponsored and funded the study; contributed to the design; and participated in the collection, analysis, and interpretation of data and in the writing, reviewing, and approval of the final publication.

References

1. Williams, H.D. Strategies to address low drug solubility in discovery and development. *Pharmacol. Rev.* **2013**, *65*, 315–499. [[CrossRef](#)] [[PubMed](#)]
2. Van Den Mooter, G. The use of amorphous solid dispersions: A formulation strategy to overcome poor solubility and dissolution rate. *Drug Discov. Today Technol.* **2012**, *9*, e79–e85. [[CrossRef](#)] [[PubMed](#)]
3. Jermain, S.V.; Brough, C.; Williams, R.O. Amorphous solid dispersions and nanocrystal technologies for poorly water-soluble drug delivery—An update. *Int. J. Pharm.* **2018**, *535*, 379–392. [[CrossRef](#)] [[PubMed](#)]
4. Lakshman, J.P.; Cao, Y.; Kowalski, J.; Serajuddin, A.T.M. Application of melt extrusion in the development of a physically and chemically stable high-energy amorphous solid dispersion of a poorly water-soluble drug. *Mol. Pharm.* **2008**, *5*, 994–1002. [[CrossRef](#)]
5. Yu, L. Amorphous pharmaceutical solids: Preparation, characterization and stabilization. *Adv. Drug Deliv. Rev.* **2001**, *48*, 27–42. [[CrossRef](#)] [[PubMed](#)]

6. Craig, D.Q.M.; Royall, P.G.; Kett, V.L.; Hopton, M.L. The relevance of the amorphous state to pharmaceutical dosage forms: Glassy drugs and freeze dried systems. *Int. J. Pharm.* **1999**, *207*, 179–207. [[CrossRef](#)] [[PubMed](#)]
7. Bernstein, J. *Polymorphism in Molecular Crystals*; Clarendon Press: Oxford, UK, 2002. [[CrossRef](#)]
8. Webster, G.K.; Pommerening, C.A.; Harman, W.W.; Gragg, M.A.; Han, J.-H.; Taylor, D.J. Exploiting Kinetic Solubility Differences for Low Level Detection of Crystallinity in Amorphous Drug Formulations. *Curr. Pharm. Anal.* **2019**, *16*, 529–538. [[CrossRef](#)]
9. Jacob, S.; Nair, A.B.; Patil, P.N.; Panda, B.P. Solid state crystallinity, amorphous state, and its implications in the pharmaceutical process. *Int. J. Pharm. Sci.* **2011**, *2*, 472–482. [[CrossRef](#)]
10. McVey, P.A.; Webster, G.K.; Galayda, K.J.; Houk, R.S. Rapid diagnosis of drug agglomeration and crystallinity in pharmaceutical preparations by electrospray laser desorption ionization mass spectrometry imaging. *J. Pharm. Biomed. Anal.* **2020**, *179*, 112977. [[CrossRef](#)] [[PubMed](#)]
11. Van Meter, M.I.; Khan, M.I.; Taulbee-Cotton, B.V.; Dimmitt, N.H.; Hubbard, N.D.; Green, A.M.; Webster, G.K.; McVey, P.A. Diagnosis of Agglomeration and Crystallinity of Active Pharmaceutical Ingredients in Over the Counter Headache Medication by Electrospray Laser Desorption Ionization Mass Spectrometry Imaging. *Molecules* **2021**, *26*, 610. [[CrossRef](#)] [[PubMed](#)]
12. Sakamoto, T.; Nakayama, K.; Fujimaki, Y.; Sasakura, D.; Kawanishi, T.; Hiyama, Y. Application of NIR spectroscopy/macrosopic mapping as a quality evaluation tool of crystal reservoir-type TDDS tapes, and an approach to high-precision qualitative prediction of API by NIR spectroscopy. *Iyakuhin Iryo Kiki Regyuratoriori Saiensu* **2010**, *41*, 971–982.
13. Fraser-Miller, S.J.; Saarinen, J.; Strachan, C.J. Vibrational Spectroscopic Imaging. In *Analytical Techniques in the Pharmaceutical Sciences. Advances in Delivery Science and Technology*; Müllertz, A., Perrie, Y., Rades, T., Eds.; Springer: New York, NY, USA, 2016. [[CrossRef](#)]
14. Haser, A.; Cao, T.; Lubach, J.; Listro, T.; Acquarulo, L.; Zhang, F. Melt extrusion vs. spray drying: The effect of processing methods on crystalline content of naproxen- povidone formulations. *Eur. J. Pharm. Sci.* **2017**, *102*, 115–125. [[CrossRef](#)] [[PubMed](#)]
15. Neilly, J.P.; Yin, L.; Leonard, S.-E.; Kenis, P.J.A.; Danzer, G.D.; Pawate, A.S. Quantitative Measures of Crystalline Fenofibrate in Amorphous Solid Dispersion Formulations by X-Ray Microscopy. *J. Pharm. Sci.* **2020**, *109*, 3078–3085. [[CrossRef](#)] [[PubMed](#)]
16. Kessner, D.; Chambers, M.; Burke, R.; Agus, D.; Mallick, P. ProteoWizard: Open Source Software for Rapid Proteomics Tools Development. *Bioinformatics* **2008**, *24*, 2534–2536. [[CrossRef](#)] [[PubMed](#)]
17. Race, A.; Styles, I.; Bunch, J. Inclusive Sharing of Mass Spectrometry Imaging Data Requires a Converter for all. *J. Proteom.* **2012**, *75*, 5111–5112. [[CrossRef](#)] [[PubMed](#)]
18. Bokhart, M.; Nazari, M.; Garrard, K.; Muddiman, D. MSiReader v1.0: Evolving Open-Source Mass Spectrometry Imaging Software for Targeted and Untargeted Analyses. *J. Am. Soc. Mass Spectrom.* **2018**, *29*, 8–16. [[CrossRef](#)] [[PubMed](#)]
19. McLafferty, F.W.; Tureček, F. *Interpretation of Mass Spectra*, 4th ed.; University Science Books, 1305 Walt Whitman Road, Suite 110: Melville, NY, USA, 1993.
20. Du, Y.; Luo, L.; Sun, S.; Jiang, Z.; Guo, X. Enantioselective separation and determination of miconazole in rat plasma by chiral LC–MS/MS: Application in a stereoselective pharmacokinetic study. *Anal. Bioanal. Chem.* **2017**, *409*, 6315–6323. [[CrossRef](#)] [[PubMed](#)]
21. Chen, Y.L.; Xie, Y.Q.; Li, L.N.; Wang, Z.T.; Yang, L. Advances in mass spectrometry imaging for toxicological analysis and safety evaluation of pharmaceuticals. *Mass Spectrom. Rev.* **2022**, *42*, 2207–2233. [[CrossRef](#)] [[PubMed](#)]

Disclaimer/Publisher's Note: The statements, opinions and data contained in all publications are solely those of the individual author(s) and contributor(s) and not of MDPI and/or the editor(s). MDPI and/or the editor(s) disclaim responsibility for any injury to people or property resulting from any ideas, methods, instructions or products referred to in the content.